Original Article

A Probabilistic Functional Atlas of the Human Subthalamic Nucleus

Wieslaw L. Nowinski,*,1 Dmitry Belov,1 Pierre Pollak,2 and Alim Louis Benabid2

1Biomedical Imaging Lab, Institute for Infocomm Research 21 Heng Hui Keng Terrace, 119613 Singapore 2University of Joseph Fourier Medical School, Grenoble, France

Abstract

This paper introduces a method for generation and validation of a probabilistic functional brain atlas of subcortical structures from electrophysiological and neuroimaging data. The method contains three major steps: (1) acquisition of pre, intra, and postoperative multimodal data; (2) selection of an accurate data set for atlas generation; and (3) generation of the atlas from the selected data set. The method is applied to construct the probabilistic functional atlas of the human subthalamic nucleus (STN). The STN atlas has been built from data collected during surgical treatment of 184 patients with Parkinson's disease. It is based on preoperative X-ray ventriculography imaging, intraoperative electrophysiological measurements and X-ray imaging, and postoperative neurological assessment. The atlas features a high resolution of 0.25 mm^3 and a high accuracy of 0.25 mm. It is dynamic and can be rapidly recalculated for arbitrary resolution and extended by adding new patient data. The atlas can easily be reformatted and warped to match patient-specific data. Its applications include planning of subthalamic stimulations and neuroscience research to study functional properties of the STN. The presented method is general and can be applied for constructing human and animal probabilistic brain atlases.

Index Entries: Probabilistic functional atlas; subthalamic nucleus; brain atlas.

Introduction

Human brain atlases play an important role in clinical, research, and educational applications (Nowinski, 2002). In particular, the importance of probabilistic brain atlases is growing recently (Mazziotta et al., 1995). An initial taxonomy of probabilistic atlases has been introduced in Nowinski et al. (2003). A probabilistic atlas can be constructed from various sources of data, such as radiological images, photographs of cryosections, literature studies, or electrophysiological measurements. Typically, a probabilistic atlas is derived from a population of data, and understanding these

*Author to whom all correspondence and reprint request should be addressed. E-mail: wieslaw@bii.a-star.edu.sg

data is a crucial part of the overall process of atlas construction. The quality of the source data impacts the accuracy of the constructed probabilistic atlas, and any errors or inaccuracies will propagate into the resulting atlas. Therefore, understanding the process of data acquisition, and particularly its limitations and sources of inaccuracies are of primary importance. Having this understanding, another critical task is validation of the data used for atlas construction. It is crucial that all data have to be checked carefully, doubtful data clarified, incorrect data rejected, and data of low quality enhanced or rejected. Therefore, we believe that atlas construction from population data cannot be decoupled from the process of data acquisition, and consequently the specific domain within which the data are acquired has also to be considered.

Microrecordings and stimulations performed during stereotactic and functional neurosurgery procedures, such as surgical treatment of Parkinson's disease (PD), are a rich source of data about the human brain. Electrophysiological data acquired for clinical purposes are also invaluable for research studies. These population (numerical) data can be converted into volumetric images, such as a probabilistic functional atlas (PFA) as we have initially proposed in Nowinski and Benabid (2002). A vast amount of electrophysiological data has been collected for the subthalamic nucleus (STN), a motor nucleus of the basal ganglia. The STN is one of the most popular target structures in surgical treatment of PD patients. Its ablation or stimulation improves the symptoms of PD. Bilateral stimulation of the STN in PD patients (Benabid et al., 1994; Benabid et al., 2000) produces a dramatic reversal in all cardinal motor signs in patients who are off their medications and gives improvements in the on-medication state.

This paper addresses the construction of the probabilistic functional atlas of the subthalamic nucleus (PFA-STN) from multimodal electrophysiological and neuroimaging data collected during surgical treatment of 184 PD patients. Data acquisition and selection are specially emphasized here and analyzed with care, which has led to a construction of a high-accuracy, high-resolution, and volumetric atlas. The method employed to construct the PFA-STN atlas is general and applicable for studying other brain structures of various species.

Material and Method

The PFA-STN (or atlas) is constructed in three major steps: (1) acquisition of preoperative, intraoperative, and postoperative multimodal data; (2) selection of a suitable data set for atlas generation; and (3) generation of the atlas from the selected data set.

Material

Material used for the construction of the PFA has been collected over many years during functional neurosurgery procedures. The aim of this kind of surgical procedure is to locate a nearly invisible small physiological target structure situated deep within the brain and accurately deliver therapy to it. Individual variations usually complicate targeting. The initial, anatomical target can be identified directly in the scan or be defined by means of a deformable brain atlas (Nowinski and Benabid, 2002). The anatomical target has then to be confirmed by electrophysiological mapping. For this purpose one or usually more electrodes are inserted into the patient's brain by using a stereotactic frame (*see* Appendix A). This electrophysiological mapping provides the functional position of structures in the brain as each structure has its own characteristic firing pattern in terms of frequency, amplitude, and shape of signal envelope. After localizing the target by microelectrode recording, the microelectrode is replaced by a permanent, deep brain simulation electrode containing four cylindrical contacts. To check and optimize the location of the target, intraoperative stimulation

Table 1
Data statistics (AC–PC intercommissural
distance, HT height of thalamus; both in mm)

Statistics	AC–PC	HT
Average length	25.85	17.45
Standard deviation of the length	1.69	1.49
Minimal length	21.67	13.20
Maximum length	29.41	20.95

is performed with neurological evaluation to test for benefit and rule out side effects. The most neurologically effective contact (the best contact) selected during surgery is further verified in a follow-up neurological assessment. By collecting data from numerous patients and verifying them clinically, a probabilistic atlas with a functional distribution of cerebral structures can be constructed and potentially new knowledge extracted from it.

The data used in our study are given in Tables 1–3. Note that the majority of patients have been operated bilaterally.

Method

Data Acquisition

Multimodal data are acquired through all stages of the procedure, i.e., pre-, intra-, and postoperatively. Preoperatively, two perpendicular projections, lateral and antero-posterior, are acquired from X-ray ventriculography (see Appendix A, Figs. A1–A3). X-ray is able to image the third ventricle (V3) from which the aterior commissure (AC), posterior commissure (PC), and height of the thalamus (HT) can be determined. The distance between the AC and PC, HT, and the width of the V3 are measured on these two preoperative projections for each patient. These values are used subsequently to normalize best contacts. Intraoperatively, the best contact is identified electrophysiologically and its position is imaged on two orthogonal X-rays. The coordinates of the best contact are measured on these two projections and reconstructed in

3D (Appendix A). Two types of quadripolar electrodes are used: DBS 3387 with 1.5 mm intercontact gap and DBS 3389 with 0.5 mm intercontact gap. The DBS's contacts have number identifiers from 0 to 3. The initial identifier of the best contact is determined during stimulation. Postoperatively, the best contact is verified neurologically during a 3-month follow-up assessment of the patient. If the contact identifier is changed, its new position can be obtained from the intraoperative X-ray images. The surgical procedure and neurological assessment have been addressed in detail in Benabid et al. (1994, 2000), and Krack et al. (2002).

Data Selection

The more the contacts used to calculate the PFA, the better it is from a statistical standpoint. However, contacts may not be accurate enough or some may even be incorrect. Therefore, a suitable balance between population and quality of data has to be maintained. Two quality criteria are applied in the process of contact selection and checking: (1) contact cluster formation and (2) height of contact reconstruction.

All the best contacts, when normalized and put together in the atlas space, form typically a cluster. Those contacts that are beyond the cluster require checking. Being beyond the cluster does not mean that the position of the contact is incorrect. It is rather interpreted as a "suspicious" position that has to be additionally checked. The contacts that were beyond the cluster had usually a wrong electrode type assigned to it, which, due to different intercontact gaps, resulted in a wrong contact positioning.

The physical height of the contact is 1.5 mm. When the contact is reconstructed accurately from two perpendicular projections, its reconstructed height (before spatial normalization) shall also be 1.5 mm. This serves as the basis for checking the accuracy of individual contacts. There are several reasons, other than a finite

Table 2
All contact data (*N* number of patients, *C* number of contacts)

Contact Type	Left Hemisphere		Right Hemisphere		Both Hemispheres	
	N	*C*	*N*	*C*	*N*	*C*
3387	5	20	5	20	5	40
3389	174	696	169	676	179	1372
Both	179	716	174	696	184	1412

Table 3
Best contact data (*N* number of patients, *C* number of contacts)

Contact Type	Left Hemisphere		Right Hemisphere		Both Hemispheres	
	N	*C*	*N*	*C*	*N*	*C*
3387	5	5	5	5	5	10
3389	174	181	169	175	179	356
Both	179	186	174	180	184	366

accuracy of calculations, that may cause the reconstructed height of contact to differ from its physical one. First, the length of the electrode measured on the projections may not be accurate enough. Second, a wrong type may be assigned to the electrode resulting in a wrong positioning of contact as electrodes have different intercontact gaps. And third, 3D reconstructions from 2D projections may not be accurate. This may be due to incorrect input parameters of the stereotactic frame (frame size, size of angiographic localizers, or projections of angiographic localizers), position of X-ray sources, or position of X-ray film plates (*see* Appendix A). This can also signal that our assumptions about patient positioning may not be met, as discussed in Appendix A. For instance, the midsagittal plane of the patient may not be parallel to the plane of the lateral projection causing distortion of the reconstructed distances.

The height of each contact was reconstructed and checked against a given range of accuracy (of +0.25 mm). If this height was beyond the range, the contact was re-examined by checking and correcting, if necessary, the electrode type, and re-measuring the electrode length on X-rays. If after these actions the height of contact was still beyond the given accuracy range, the contact was rejected. As a result, a small amount of contacts (below 3%) where reconstructed height was lower than 1.25 mm or higher than 1.75 mm were rejected.

Atlas Generation

From the selected set of best contacts, the atlas was generated in four steps: (1) reconstruction of parameters for contact normalization, (2) contract normalization, (3) voxelization of normalized contacts, and (4) calculation of atlas function as frequency of best contacts. Data normalization is based on the landmarks determined during surgery planning, namely, AC, PC, HT, and V3. Consequently, the coordinates of each best contact are scaled antero-posteriorly proportionally to the intercommissural distance AC–PC and dorso-ventrally proportionally to

the height of thalamus HT. Lateral compensation against the width of the third ventricle by shifting its lateral coordinate by $V3_{average} - V3)/2$, performed usually for the ventrointermediate nucleus of the thalamus, was not applied here, as the STN is mostly situated below the level of the third ventricle (comparison between the functional STN calculated with and without lateral compensation was done in Nowinski et al., *submitted*).

To normalize a contact, its location (represented here by the superior and inferior points on its axis) as well as the AC–PC and HT are required. These values are not given explicitly and they have to be estimated from two sets of X-ray projections: the AC–PC and HT from ventriculography acquired preoperatively, and the position of the electrode with its four contacts taken intraoperatively after electrophysiological confirmation. Under assumption that the midsagittal plane is parallel to the lateral plane, the AC–PC and HT can be measured directly on the lateral projection and V3 on the anteroposterior projection. The calculation of 3D coordinates of a point from its two 2D orthogonal projections is theoretically simple. However, in our case this problem has to be considered in the given stereotactic environment taking into account potential errors that may occur due to mis-positioning of patient. Two reconstruction methods along with error analysis are given in Appendix A. The first method is more practical (though resulting in an error of about 0.1 mm) as it allows us to make measurements against anatomical landmarks, such as the AC or PC.

Each best contact is normalized by applying the corresponding patient-specific normalization parameters and then placed in the common atlas space. The normalized best contacts are subsequently voxelized. A rapid and optimal algorithm for contact voxelization is given in Nowinski et al. (2003). The atlas function in a given point is defined as plurality of best contacts at this point. In a given voxel, the (discretized) atlas function is calculated by counting the number of best contacts in this voxel. Finally, atlas probability is computed as a linear function (specified by a user) of the atlas function.

Results

PFA-STN Calculation

The PFA-STN has been calculated with 0.25 mm^3 resolution and 0.25 mm accuracy. Figure 1 shows the normalized STN best contacts (A) and 3D voxelized PFA-STN (B). Figure 2 shows coronal and sagittal sections through the PFA-STN displayed as gray scale images located in the stereotactic space based on the mid-commissural point (the midpoint between the AC and PC). The PFA-STN is easily deformable in 3D and can be superimposed on patient-specific data. For instance, Fig. 3 shows the PFA-STN overlaid a coronal MRI slice (this image is generated from Nowinski et al. [2005]).

Validation

The key component of the PFA algorithm is voxelization of a deformed cylinder detailed in Nowinski et al. (2003). Despite theoretical correctness proven, its implementation (language, run-time libraries, platform, and so on) may impact the resulted PFA. As correctness of medical applications is particularly critical, it is crucial to validate the software implementation of cylinder voxelization. A cylinder representing a stereotactic contact may vary in terms of size, position, direction, and scaling. As the number of combination of all parameter values is enormous, the software implementation of voxelization has been validated by using the Monte Carlo method. The formula estimating the probability of error in function of the number of Monte Carlo tests has been derived in Appendix B. Based on this formula we have checked 1 million randomly generated cylinders from a wide range of parameters and
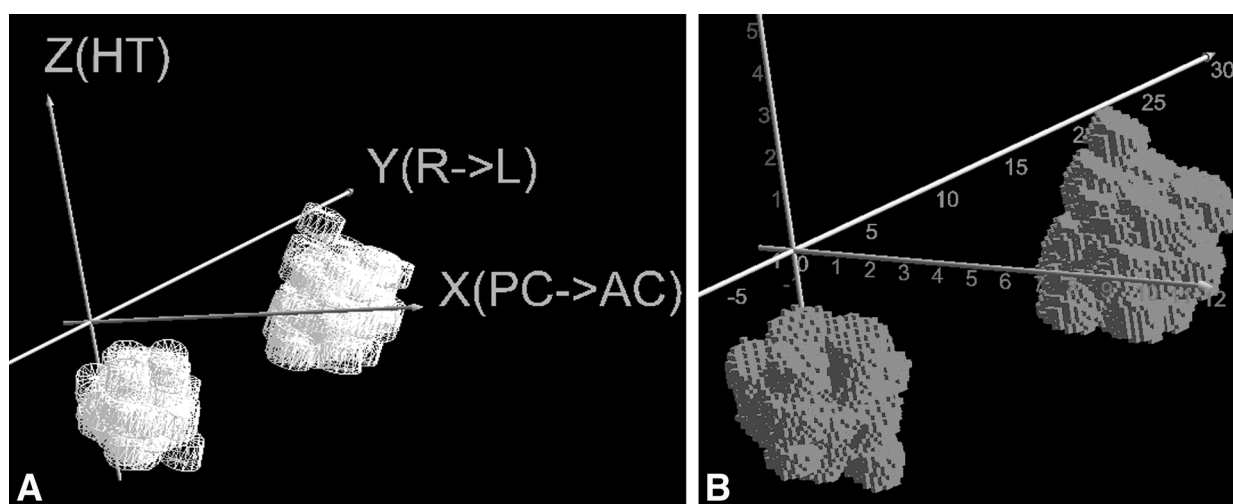
Fig. 1. 3D PFA-STN: **(A)** normalized best contacts (the axes are labeled); **(B)** voxelized PFA-STN (the marks on *Y*-axis are in millimeters; the unit for each of *X* [in AC–PC units] and *Z* [in HT units] axis corresponds to 2 mm).

with the significance level of $\varepsilon = 0.01$ obtained no errors. This guarantees 0.99 probability of the correctness of algorithm implementation.

Discussion

The constructed PFA-STN is the result of a long-term and tedious effort. The collection of these unique data used for atlas construction took several years. The parameters of stereotactic contacts and the values of scaling factors have been carefully checked first manually and then automatically. A dedicated tool has been developed to display and manipulate the contacts and to provide two-way correspondence between the list of contacts and their 3D models (Nowinski et al., 2002).

The resulting PFA-STN, based on electrophysiology and neuroimaging, is to our best knowledge the first and only so far volumetric electrophysiology-based brain atlas. The closest effort is the development of a database of best point targets collected from therapeutic lesioning (Finnis et al., 2000), based on a coding structure from Tasker et al. (1978). Besides being novel, our atlas has several

advantages. It is volumetric and isotropic, which enables its reformatting in any plane and facilitates its 3D warping. The atlas has a high resolution of 0.25 mm^3 and accuracy of 0.25 mm making it much accurate for targeting than MRI (Saint-Cyr et al., 2002) or electronic versions of print atlases (Nowinski, 2001). In fact, atlas resolution is user-defined; however, calculating the PFA-STN with a higher resolution than 0.25 mm^3 does not make sense as the data accuracy threshold is 0.25 mm. We are not aware of any other brain atlas constructed with such high accuracy as our PFA-STN.

The high quality of the obtained PFA-STN is the result of a meticulous analysis. Understanding the surgical procedure, the stereotactic environment for data acquisition, and the sources of errors and inaccuracy were critical. Two major sources of potential errors analyzed here were the data acquisition process and the algorithm for PFA generation. Data acquisition is complicated and is being done in three stages. Errors may occur during data collection as well as their archival. The accuracy of
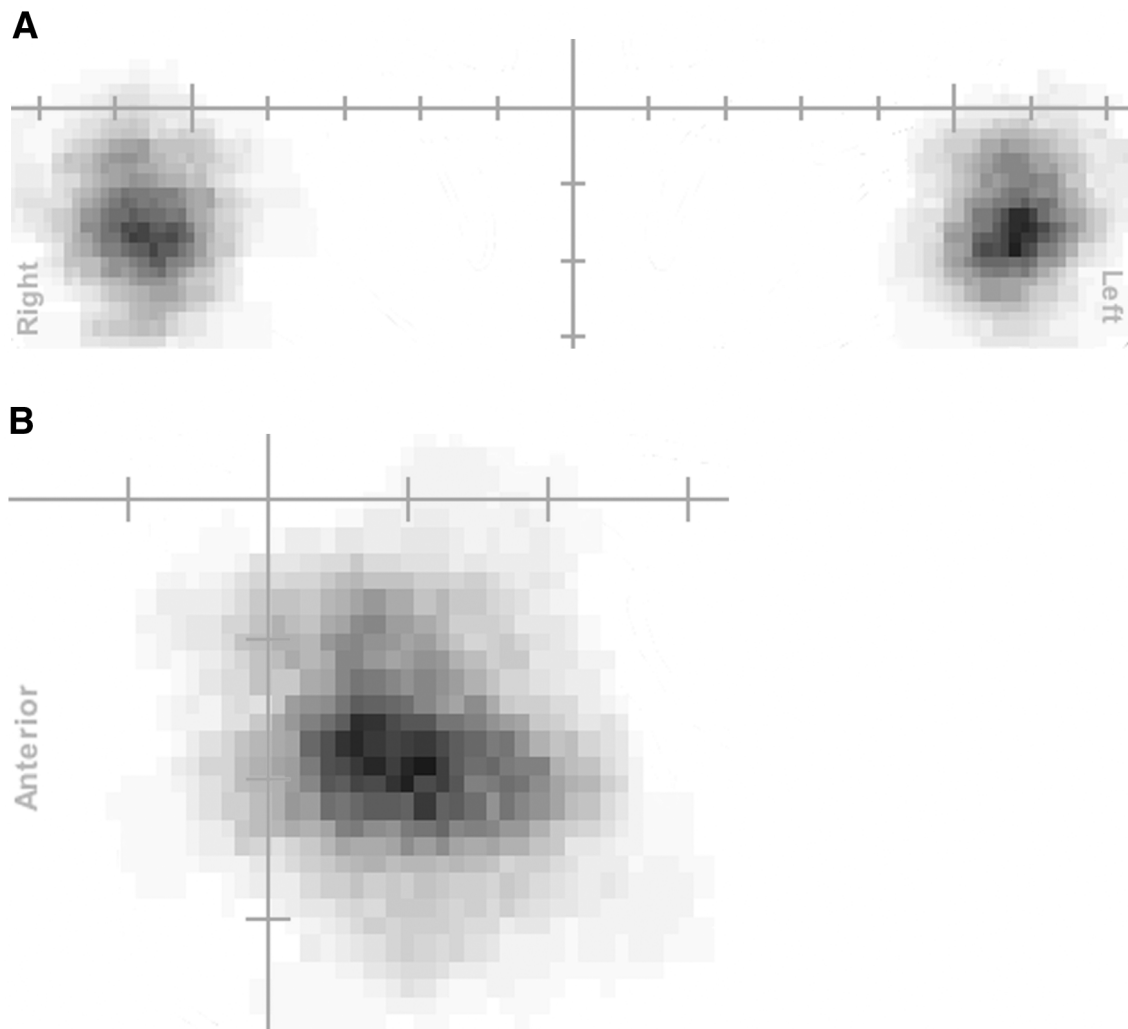
A

B

Fig. 2. PFA-STN: **(A)** coronal section; **(B)** sagittal section. The white color corresponds to zero probability, the black color to probability equal to one, and the gray scale is proportional to probability. The center of the coordinate system is at the midcommissural point and the marks on the axes are placed at every 2 mm.

preoperative and intraoperative X-rays depends on the stereotactic environment (location of X-ray sources and film plates) as well as patient positioning and frame fixation. The accuracy of 3D coordinates of the landmarks and contacts is dependent on the accuracy of mensuration of the X-rays and accuracy of the reconstruction method (estimated in Appendix A). Simple errors may also occur during archival of hundreds of contacts including their identifiers, type of electrodes, and positions as well as the corresponding landmarks. Contact cluster formation and contact height reconstruction were two main criteria used for contact selection and checking. The second source of potential inaccuracies is the algorithm for PFA generation. As its correctness was previously proven theoretically, in this work we have focused on validation of the software implementation of contact voxelization. This implementation was validated by means of the Monte Carlo method with 0.99 probability of correctness.
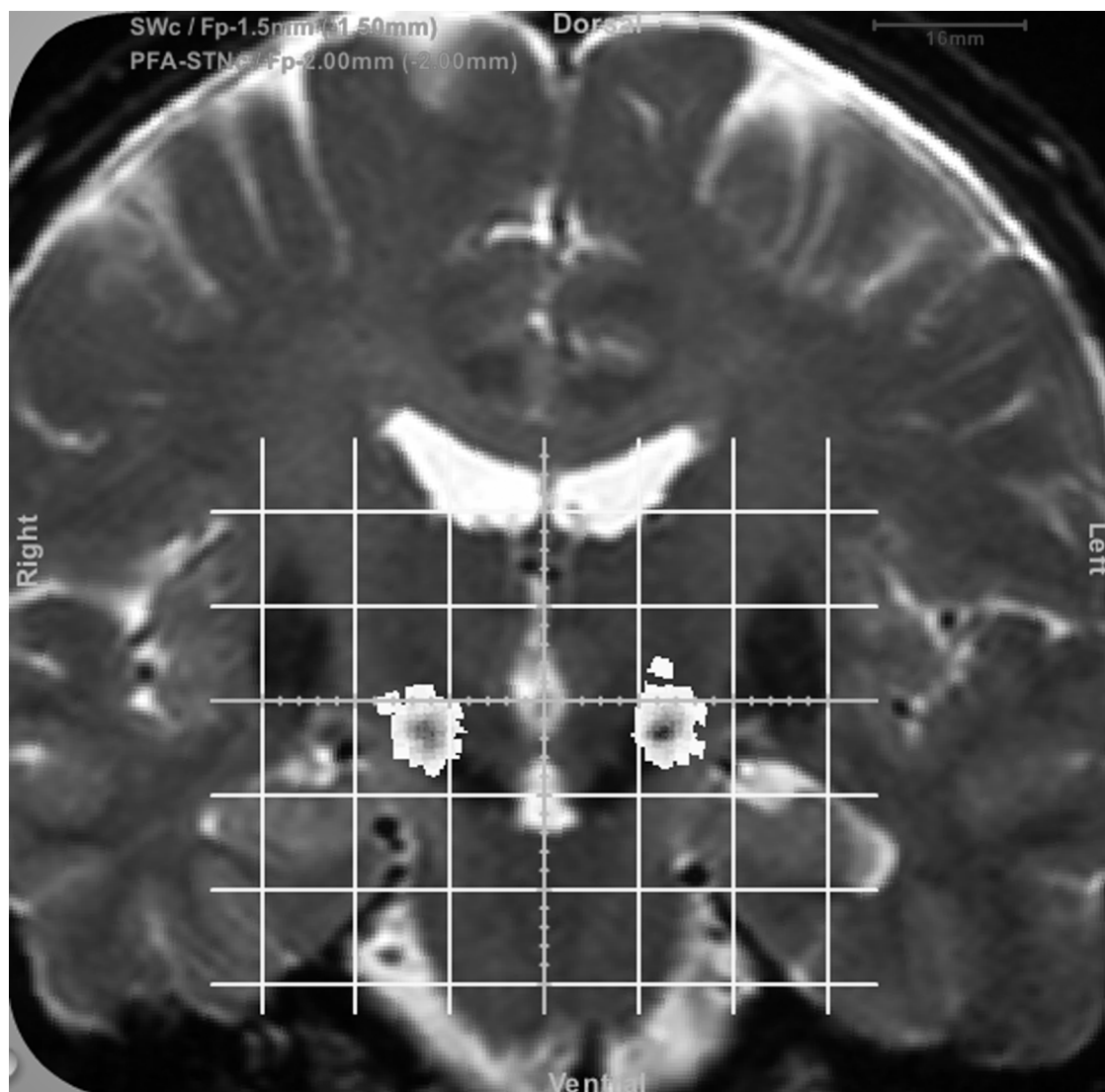
Fig. 3. Deformable PFA-STN overlaid on a T_2-weighted MRI coronal image. The rectangular grid has 10 mm spacing.

Several limitations of the constructed PFA-STN result from data acquisition and the PFA algorithm. The data used to calculate the PFA-STN have been acquired for PD patients only, not for normals, as the procedure is invasive. The algorithm is limited to the electrodes with the cylindrical contacts and models the activation region to correspond to the shape of the contact, which is a simplification. The linear spatial contact normalization is theoretically inferior to nonlinear warping (Toga, 1998). However, practically, within the region between the AC and PC where the STN is located, the difference between the linear and nonlinear warping is negligible (Grachev et al., 1999). A ventral scaling based on the height of the thalamus is not accurate. An antero-posterior scaling may be correlated better to other than the AC or PC landmarks in the region around the floor of the third ventricle.

The direct application of this work is for targeting in subthalamic stimulation as the PFA-STN provides the best target (i.e., any point in the atlas with the highest probability may be chosen as the best target). For this purpose, the PFA-STN has been co-registered with an anatomical atlas (Schaltenbrand and Wahren, 1977) and incorporated in the extended edition of *The Cerefy Clinical Brain Atlas* (Nowinski et al., 2005) making it available both to neurosurgical and neuroscience communities. The PFA-STN can also be useful in neuroscience research to study properties of functional structures from a probabilistic standpoint. For instance in Nowinski et al. submitted), we have analyzed the PFA-STN in terms of probability distribution versus corresponding volume and identified two components in the STN as well as observed differences between the left and right STN. As the method is general, it is applicable to other than the STN structures and can handle other neuroimage acquisition techniques. The algorithm for PFA generation is very fast and it is also available publicly (www.cerefy.com) along with a portal for best contact deposition (Nowinski et al., 2002). Consequently, the community can use it to generate human and animal probabilistic atlases over the Internet. In addition, the position of the best contact and its normalization parameters can also be obtained from other imaging modalities, for instance, directly from volumetric MRI and CT acquisitions. However, geometric distortion in case of MRI and postoperative edema (on a postoperative scan showing the position of the best contact) may limit the accuracy of the resulting atlas.

In conclusion, the PFA of the human STN is derived from 366 stereotactic best contacts of 184 PD patients. The atlas is volumetric and of high-resolution (0.25 mm^3) and its accuracy is 0.25 mm. It is based on electrophysiology, neuroimaging, and neurological assessment. The atlas can easily be reformatted and warped to match patient-specific data. This is a dynamic atlas that can easily be extended by adding new data. Its applications include planning of subthalamic stimulations as well as neuroscience research to study functional properties of the STN. The presented method is general and can be applied for constructing human and animal probabilistic brain atlases.

Acknowledgments

References

Benabid, A. L., Koudsie, A., Benazzouz, A., et al. (2000) Subthalamic stimulation for Parkinson's disease. Arch. Med. Res. 31(3), 282–289.

Benabid, A. L., Pollak, P., Gross, C., et al. (1994) Acute and long-term effects of subthalamic nucleus stimulation in Parkinson's disease. Stereotact. Funct. Neurosurg. 62(1–4), 76–84.

Grachev, D., Berdichevsky, D., Rauch, S. L., et al. (1999) A method for assessing the accuracy of intersubject registration of the human brain using anatomic landmarks. Neuroimage 9(2), 250–268.

Finnis, K. W., Starreveld, Y. P., Parrent, A. G., and Peters, T. M. (2000) A 3-dimensional database of deep brain functional anatomy, and its application to image guided neurosurgery. In: Third International Medical Image Computing and Computer Aided Intervention Conference, MICCAI 2000, Pittsburgh, PA, Oct 11–14, pp. 1–8.

Krack, P., Fraix, V., Mendes, A., Benabid, A.L., and Pollak, P. (2002) Postoperative management of subthalamic nucleus stimulation for Parkinson's disease. Mov. Disord. 17 Suppl. 3, S188–S197.

Mazziotta, J. C., Toga, A. W., Evans, A. C. (1995) A probabilistic atlas of the human brain: theory and rationale for its development. NeuroImage 2, 89–101.

Nowinski, W. L. (2001) Computerized brain atlases for surgery of movement disorders. Semin. Neurosurg. 12(2), 183–194.

Nowinski, W. L. (2002) Model enhanced neuroimaging: clinical, research, educational applications. In: Yearbook of Medical Informatics, pp. 132–144.

Nowinski, W. L., Belov, D., Benabid, A. L. (2002) A community-centric Internet portal for stereotactic and functional neurosurgery with a probabilistic
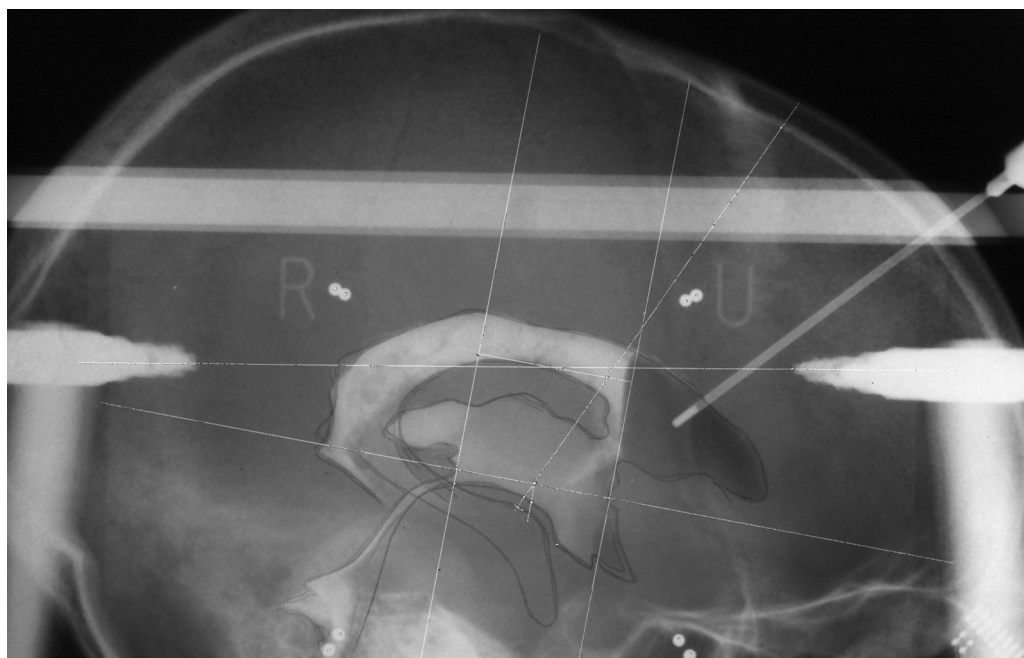
Fig. A1. An X-ray showing the lateral view. The line passing through the AC and PC and another line marking the height of thalamus are drawn.

functional atlas. Stereotact. Funct. Neurosurg. 79, 1–12.

Nowinski, W. L., Belov, D., Benabid, A. L. (2003) An algorithm for rapid calculation of a probabilistic functional atlas of subcortical structures from electrophysiological data collected during functional neurosurgery procedures. NeuroImage 18, 143–155.

Nowinski, W. L., Belov, D., Pollak, P., Benabid, A. L. Statistical analysis of 168 bilateral subthalamic stimulations by means of the probabilistic functional atlas. Neurosurgery, submitted.

Nowinski, W. L. and Benabid, A. L. (2002) New directions in atlas-assisted stereotactic functional neurosurgery. In: Advanced Techniques in Image-Guided Brain and Spine Surgery. Germano, I. M. (ed). Thieme, New York, pp. 162–174.

Nowinski, W. L., Thirunavuukarasuu, A., Benabid, A. L. (2005) The Cerefy Clinical Brain Atlas. Extended Edition With Surgery Planning and Intraoperative Support. Thieme, New York.

Saint-Cyr, J. A., Hoque, T., Pereira, L. C., et al. (2002) Localization of clinically effective stimulating electrodes in the human subthalamic nucleus on magnetic resonance imaging. J. Neurosurg. 97(5), 1152–1166.

Schaltenbrand, G. and Wahren, W. (1977) Atlas for Stereotaxy of the Human Brain. Thieme, Stuttgart.

Tasker, R. R., Hawrylyshyn, P., Organ, W. (1978) Computerized graphic display of physiological data collected during human stereotactic surgery. Appl. Neurophysiol. 41, 187–193.

Toga A. W. (ed.) (1998) Brain Warping. Academic, San Diego.

Appendix A: 3D Reconstruction From Two 2D Projections in a Stereotactic Environment

The landmarks and coordinates of best contacts are measured on X-rays. Figure A1 shows a sample X-ray.

Coordinate System

We introduce a 3D system of coordinates where the position of the X-ray sources, $(-S_s,0,0)$ and $(0,-S_c,0)$, stereotactic frame $F \times F \times F$, and image plates $(I_s,0,0)$ and $(0,I_c,0)$ are shown in Figs. A2 and A3. The problem of reconstruction of the electrodes and patient landmarks can be
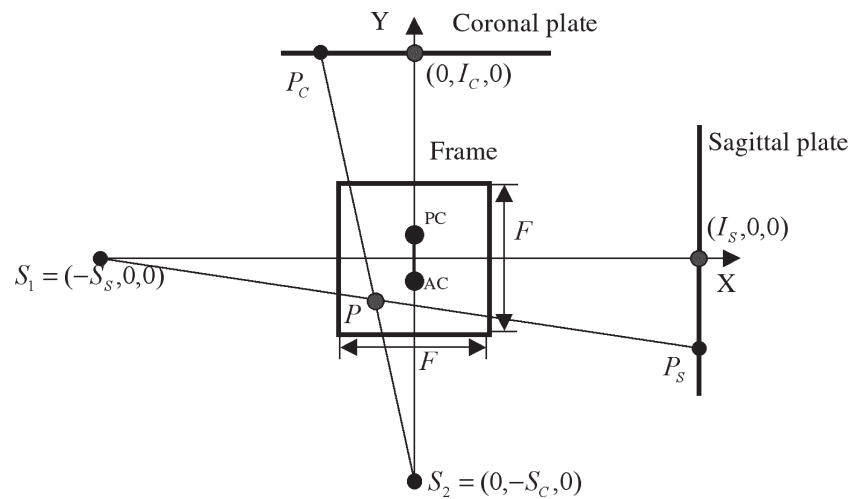
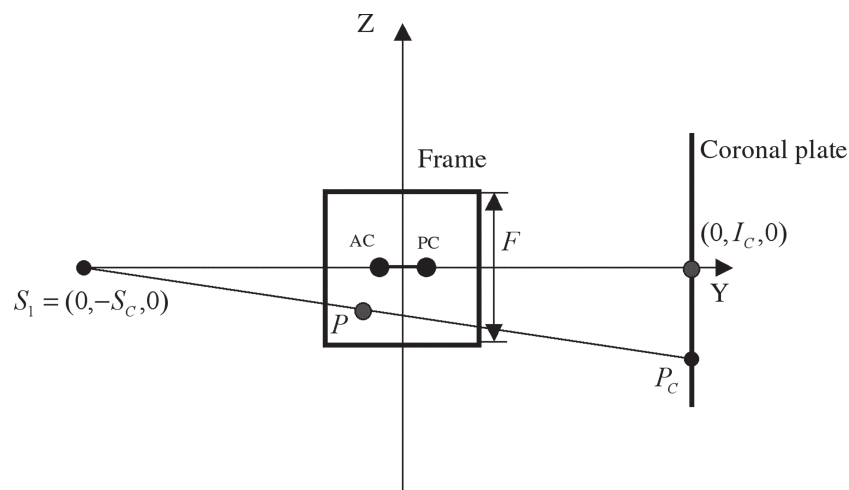Fig. A2. Axial view of the coordinate system.

Fig. A3. Sagittal view of the coordinate system.

reduced to that of reconstruction point $P = (x, y, z)$ from its two orthogonal projections $P_s = (x_s, y_s, z_s)$ and $P_c = (x_c, y_c, z_c)$, namely, sagittal (lateral) and coronal (antero-posterior), respectively, Figs. A2 and A3.

We assume that the center of patient's AC–PC line is the center of the coordinate system and segment (AC, PC) lies on Y-axis. Under these assumptions we can measure projections of electrodes and landmarks against the projection of the PC or AC and then reconstruct them in 3D space.

Method 1: Scaling Factor Reconstruction

Consider the sagittal view of the coordinate system, Fig. A4. As we are interested in the active area of angiographic localizers $2f \times 2f$ ($2f < F$), we consider the point inside the stereotactic
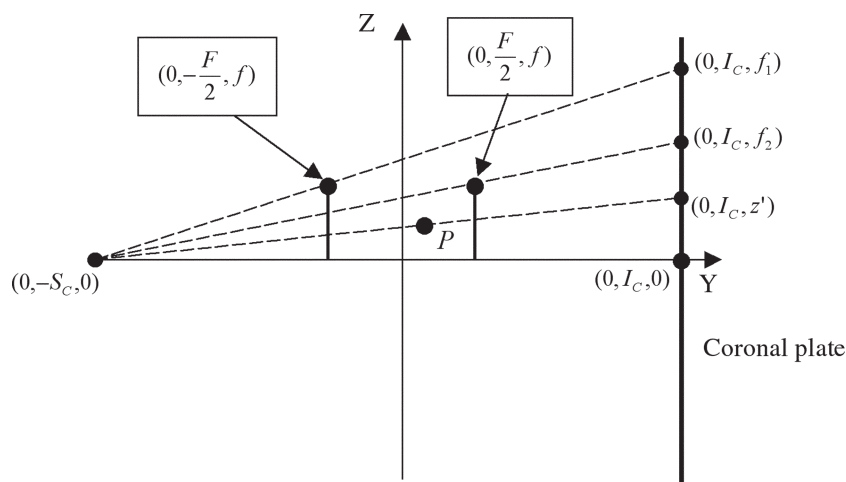
Fig. A4. Illustration of a scaling reconstruction method.

frame $P = \left(0, -\dfrac{F}{2} + tF, \beta f\right)$, where $t \in [0,1], \beta \in [-1,1]$.

Using X-ray images we can find f_1 and f_2 (Fig. A5).

As a result we get $\alpha_1^c = \dfrac{f}{f_1}$ and $\alpha_2^c = \dfrac{f}{f_2}$. Let us

take $\alpha_1^c \leq \alpha^c \leq \alpha_2^c$ and $t = \dfrac{(\alpha^c - \alpha_1^c)}{\alpha_2^c - \alpha_1^c}$. Assume that

$$\beta f = \alpha^c z' \qquad (A1)$$

By using similarity of triangles we have

$$\beta f = \dfrac{z'\left(tF - \dfrac{F}{2} + S_c\right)}{I_c + S_c} \qquad (A2)$$

To check assumption (A1) let us explore this difference:

$$\alpha^c z' - \dfrac{z'\left(tF - \dfrac{F}{2} + S_c\right)}{I_c + S_c}$$

$$= z' \dfrac{\alpha^c(I_c + S_c) - tF + \dfrac{F}{2} - S_c}{I_c + S_c} = \lambda$$

Obviously λ is changing monotonically when α^c is changing from α_1^c to α_2^c. Hence, we get the following condition for λ:

$$\alpha^c = \alpha_1^c, \ t = 0: \ \lambda_1 = z_1' \dfrac{\alpha_1^c(I_c + S_c) + \dfrac{F}{2} - S_c}{I_c + S_c}$$

$$\alpha^c = \alpha_2^c, \ t = 1: \ \lambda_2 = z_2' \dfrac{\alpha_2^c(I_c + S_c) - F + \dfrac{F}{2} - S_c}{I_c + S_c} \qquad (A3)$$

$$|\lambda| \leq \max\left(|\lambda_1|, |\lambda_2|\right)$$

By considering conditions in an operating room, we get (all values are in mm):

$$F = 274, f = \dfrac{60}{2}, \alpha_1^c = \dfrac{60}{66.02}, \alpha_2^c = \dfrac{60}{60.61},$$

$$I_c = 171, S_c = 3210, z_1' = \dfrac{66.02}{2}, z_2' = \dfrac{60.61}{2},$$

$$\lambda_1 = -0.00288, \lambda_2 = -0.00025$$

So we can take $|\lambda| \approx 0.0$ and our assumption (A1) causes the error in the reconstructed data of 10^{-2} mm, which is acceptable in stereotactic and functional neurosurgery. A similar assumption for the sagittal X-ray source gives:

$$\alpha_1^s \leq \alpha^s \leq \alpha_2^s$$
$$\alpha_1^c \leq \alpha^c \leq \alpha_2^c$$
$$x = x_c \alpha_c \qquad (A4)$$
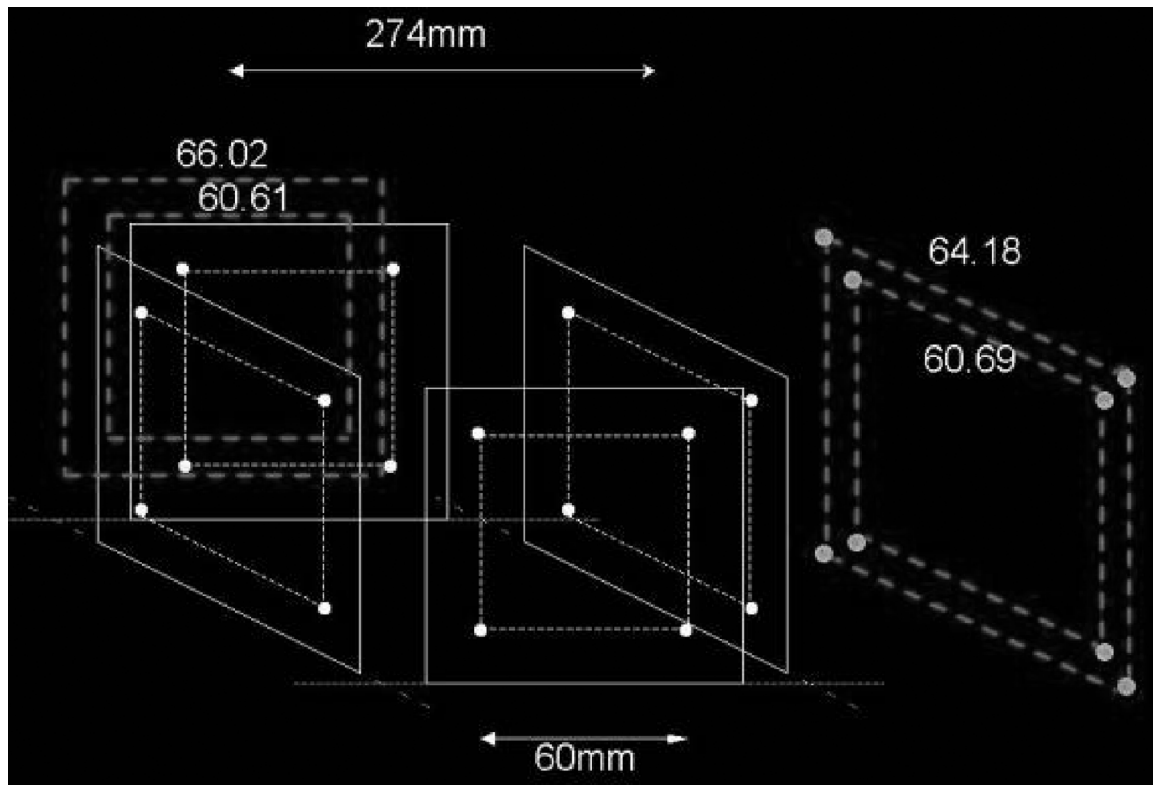$$y = y_s \alpha_s$$
$$z = z_s \alpha_s$$

Fig. A5. X-ray films with projections of the angiographic localizers.

Thus, for given $\alpha_1^s \leq \alpha^s \leq \alpha_2^s$ and $\alpha_1^c \leq \alpha^c \leq \alpha_2^c$, we can reconstruct point P from its two projections $P_s = (x_s, y_s, z_s)$ and $P_c = (x_c, y_c, z_c)$ by solving the following system of equations:

$$\alpha_1^s \leq \alpha^s \leq \alpha_2^s$$
$$\alpha_1^c \leq \alpha^c \leq \alpha_2^c$$
$$x = x_c \alpha^c$$
$$t = \frac{x + \dfrac{F}{2}}{F} \in [0,1] \qquad (A5)$$
$$\alpha^s = \alpha_1^s(1-t) + \alpha_2^s t$$

$$y = y_s \alpha^s$$
$$z = z_s \alpha^s$$

Unfortunately, solution of (A5) is not unique and we have to make additional assumption:

$$\alpha^c = \frac{\alpha_1^c + \alpha_2^c}{2} \qquad (A6)$$

Under assumption (A6), equation (A5) has a unique solution.

The main advantage of this method is that reconstruction does not require the assumption about position of AC–PC. Indeed because of (A1), the distance between points P_1 and P_2 equals to , $\alpha \, |P_1'P_2'|$ where a is the same for P_1 and P_2 (Fig. A6).

The main disadvantage of this approach is that it uses assumption (A6). Let us analyze the average reconstruction error caused by (A6). We have:

- α—unknown scaling factor,

- α—assumed by (A6), scaling factor $\alpha' = 0.949376$.

Let us take an average value of AC–PC as 24 mm; then y coordinate of the point belongs to [–12,12]. It gives us estimation for α as $\mu_1 \leq \alpha \leq \mu_2$, where

$$t_1 = \frac{-12 + \dfrac{F}{2}}{F} = 0.456204,$$
$$\mu_1 = \alpha_1^c(1-t_1) + \alpha_2^c t_1 = 0.945823$$
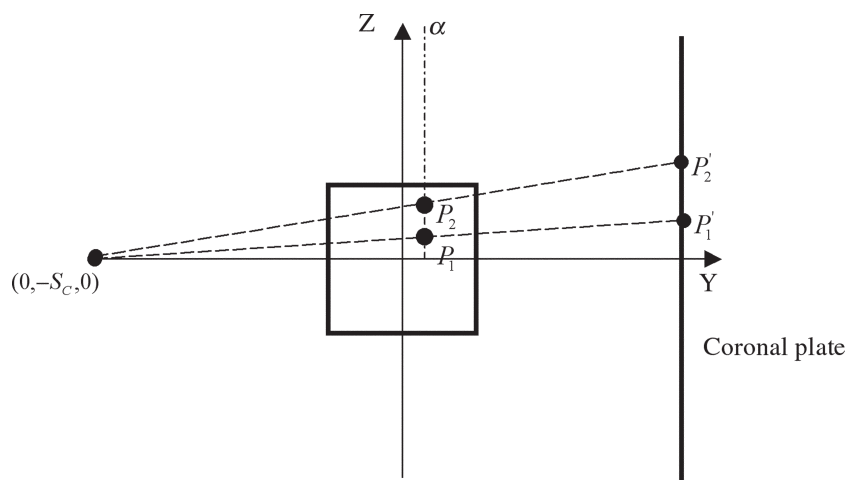
Fig. A6. Distance between points P_1 and P_2 equals to $\alpha \left| P_1' P_2' \right|$.

and

$$t_2 = \frac{-12 + \dfrac{F}{2}}{F} = 0.543796,$$

$$\mu_2 = \alpha_1^c(1 - t_2) + \alpha_2^c t_2 = 0.952928$$

Then

$$\left| \alpha - \alpha' \right| \le \Psi = \mu_2 - \alpha' = 0.003553$$

and

$$\left| z'\alpha - z'\alpha' \right| \le \left| z' \right| \Psi \le \frac{66.02}{2} \times 0.003553 = 0.117275 \text{ mm.}$$

Thus, assumption (A6) causes an average reconstruction error as approx 0.1mm, which is acceptable in stereotactic and functional neurosurgery.

Method 2: Geometrical Reconstruction

This approach basically finds intersection P of two lines $S_1 P_s$ and $S_2 P_c$ (Fig. A2). For this purpose, we need to know all six coordinates. Assume that only three of them are known, for example: $P_s = (?, y_s, z_s)$ and $P_c = (x_c, ?, ?)$. We demonstrate that in this case, point P can be reconstructed. Let us consider this reconstruction in three steps:

1. From coordinates x_c and y_s, we find x, y coordinates of P as a result of intersection of two lines l_1 and l_2 (Fig. A7).
2. From the previous step we calculate the length of segment $S_1 A$ (Fig. A8).
3. From similarity of triangles $\Delta S_1 AP$ and $\Delta S_1 BP_s$ we find z coordinate of P (Fig. A8).

In more details we get:

Step 1. Equation of line l_1:

$$L_1 = \sqrt{(I_S + S_S)^2 + y_S^2}$$

$$e = (e_x, e_y) = \frac{1}{L_1}(I_s + S_s, y_s)$$

$$\begin{cases} x = -S_s + e_x t_1 \\ y = e_y t_1 \\ t_1 \in [-\infty, +\infty] \end{cases}$$

Equation of line l_2:

$$L_2 = \sqrt{x_C^2 + (I_C + S_C)^2}$$

$$f = (f_x, f_y) = \frac{1}{L_2}(x_c, I_c + S_c)$$

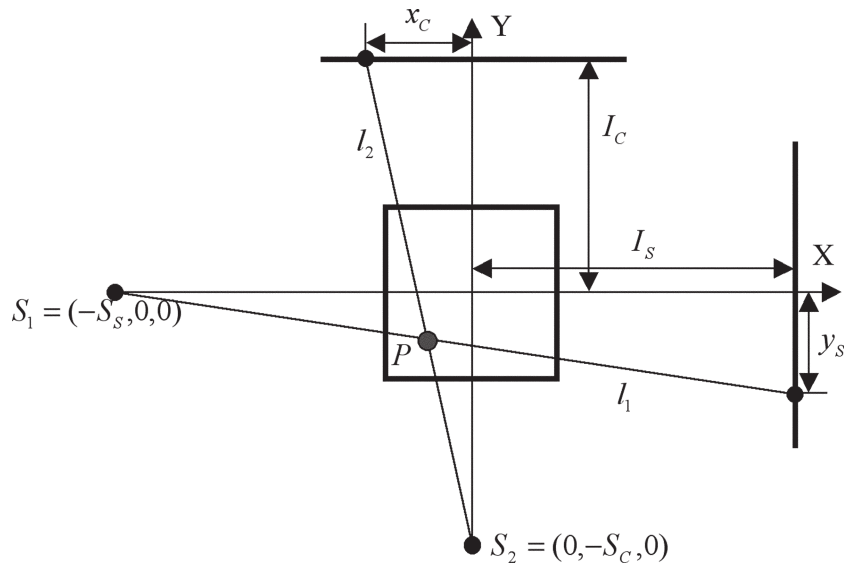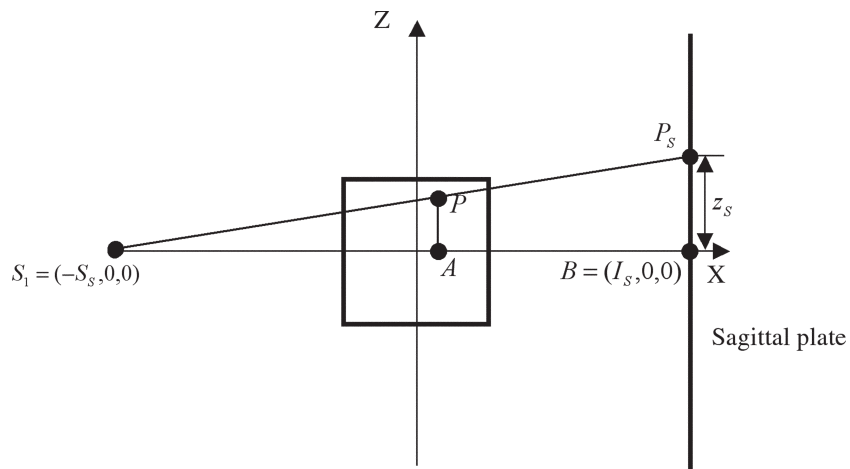$$\begin{cases} x = f_x t_2 \\ y = -S_c + f_y t_2 \\ t_2 \in [-\infty, +\infty] \end{cases}$$

Find x, y:

Fig. A7. Step 1 (top 2D view).

Fig. A8. Steps 2 and 3 (view from X-ray source S_2).

$$\begin{cases} -S_c + e_x t_1 = f_x t_2 \\ e_y t_1 = -S_c + f_y t_2 \end{cases}$$

$$t_2 = \frac{-e_x S_c - e_y S_s}{e_y f_x - e_x f_y}$$

$$\begin{cases} x = f_x t_2 \\ y = -S_c + f_y t_2 \end{cases}$$

Step 2. Find $|S_1 A|$:

$$A = (x, y, 0)$$

$$|S_1 A| = \sqrt{(x + S_s)^2 + y^2}$$

Step 3. Find z:

$$\frac{z}{z_s} = \frac{|S_1 A|}{|S_1 B|}$$

$$z = z_s \frac{|S_1 A|}{I_s + S_s}$$

The advantage of this approach is that it is accurate. But this accuracy is fully relied on the assumption of AC–PC location. This assumption can be avoided if we measure coordinates against a projection of the center of our 3D coordinates. This projection can be found from the projections of the angiographic localizers (Fig. A5).

Appendix B: Validation of the Voxelization Procedure

For a given cylinder, let *L* be the list of voxels each having its center inside the cylinder. We analyze two types of possible errors: external and internal.

Definition 1. If (x, y, z) belongs to the cylinder but $(x, y, z) \in L$, then an *external error* occurs in (x, y, z).

Definition 2. If (x, y, z) does not belong to the cylinder but $(x, y, z) \notin L$, then an *internal error* occurs in (x,y,z).

In a general case, a program using Definitions 1 and 2 has to check all possible cylinders described by the following parameters:

$$\text{size: } \begin{cases} r \in [r_1, r_2] \\ h \in [h_1, h_2] \end{cases}$$

$$\text{inferior tip position: } \begin{cases} x \in [x_1, x_2] \\ y \in [y_1, y_2] \\ z \in [z_1, z_2] \end{cases}$$

$$\text{direction of the cylinder axis: } \begin{cases} \varphi \in [\varphi_1, \varphi_2] \\ \theta \in [\theta_1, \theta_2] \end{cases}$$

$$\text{scaling on } x, y, z \text{ axis: } \begin{cases} S_x \in [S_{x1}, S_{x2}] \\ S_y \in [S_{y1}, S_{y2}] \\ S_z \in [S_{z1}, S_{z2}] \end{cases}$$

Checking directly all possible combinations of these parameters requires an enormous amount of time. The use of the Monte Carlo method speeds up this process. Then, for each simulation trial, a cylinder with uniformly distributed parameters is voxelized and checked against Definitions 1 and 2.

Let us consider some cylinder parameter $t \in [t_1, t_2]$. Assume that there is a set of ranges E such that $E \subset [t_1, t_2]$ and if $t \in E$, then an internal or external error occurs. Let us estimate the number of Monte Carlo tests in which E is hit at least once. Then, as t is uniformly distributed on $[t_1, t_2]$, probability $p\ (t \in E) = \dfrac{L_E}{(t_2 - t_1)}$, where L_E is the sum of the lengths of all ranges from E. L_E is unknown for any $t \in [t_1, t_2]$, but we can choose some value d_t approximating $\dfrac{L_E}{(t_2 - t_1)}$. Then, by using d_t we can esti mate the number of Monte Carlo tests in which E is hit at least once and at the same time this estimation will have error $0 \leq d_t \leq 1$. If after running this number of Monte Carlo tests we get zero internal and external errors, then we are sure with probability $1 - d_t$ that the implementation is correct (and we are sure with probability d_t that the implementation may be incorrect).

Let N be the number of Monte Carlo tests. By using the schema of Bernoulli's trials, we estimate the probability of not hitting at least one error set, where the error of this approximation is $\varepsilon = \max(d_r, d_h, d_x, d_y, d_z, d_\varphi, d_\theta, d_{S_x}, d_{S_y}, d_{S_z})$ (the significance level). Hence, we get:

$$p = (1-d_r)(1-d_h)(1-d_x)(1-d_y)(1-d_z)(1-d_\varphi)(1-d_\theta) \\ \times (1-d_{S_x})(1-d_{S_y})(1-d_{S_z})$$

$$q = 1 - p$$

$$p(A) = \frac{N!}{K!(N-K)!} p^k q^{N-K}$$

where p is the probability of not hitting at least one error set in one test, A is an event of not hitting any error set $K = N$ times, and $P(A)$ is a probability that the event A will happen K times in N trials. All events are supposed to be independent. Hence we get:

$P(A) = ((1-d_r)(1-d_h)(1-d_x)(1-d_y)(1-d_z) (1-d_\varphi)$
$\times (1-d_\theta)(1-d_{S_x})(1-d_{S_y})(1-d_{S_z}))^N$

In addition, we have to check the arbitrary combinations of the error sets. From the properties of affine transformations it follows that there are only four independent combinations for size (r, h), position (x, y, z), direction (φ, θ), and scaling (S_x, S_y, S_z), corresponding to events $P(B_{size}) = (1-d_r, d_h)^N$, $P(B_{position}) = (1-d_x d_y d_z)^N$, $P(B_{direction}) = (1-d_\varphi d_\theta)^N$, and

$P(B_{scaling}) = (1-d_{S_x} d_{S_y} d_{S_z})^N$. The number of Monte Carlo N trials is selected such that

$P = \max (P(A), P(B_{size}), P(B_{position}), P(B_{scaling})) \rightarrow 0.$

We have checked 1 million randomly generated cylinders from a wide range of parameters and obtained zero internal or external errors with a significance level of $\varepsilon = 0.01$. This guarantees 0.99 probability of the correctness of implementation.